



HAL
open science

Measuring Electrical Resistivity at the Nanoscale in Phase-Change Materials

L. Zhang, Frédéric Lorut, Kilian Gruel, Martin Hÿtch, Christophe Gatel

► **To cite this version:**

L. Zhang, Frédéric Lorut, Kilian Gruel, Martin Hÿtch, Christophe Gatel. Measuring Electrical Resistivity at the Nanoscale in Phase-Change Materials. *Nano Letters*, 2024, 24 (19), pp.5913-5919. 10.1021/acs.nanolett.4c01462 . hal-04727906

HAL Id: hal-04727906

<https://hal.science/hal-04727906v1>

Submitted on 4 Dec 2024

HAL is a multi-disciplinary open access archive for the deposit and dissemination of scientific research documents, whether they are published or not. The documents may come from teaching and research institutions in France or abroad, or from public or private research centers.

L'archive ouverte pluridisciplinaire **HAL**, est destinée au dépôt et à la diffusion de documents scientifiques de niveau recherche, publiés ou non, émanant des établissements d'enseignement et de recherche français ou étrangers, des laboratoires publics ou privés.

Measuring electrical resistivity at the nanoscale in phase change materials

Leifeng Zhang,¹ Frédéric Lorut², Kilian Gruel¹, Martin J. Hÿtch^{1*}, Christophe Gatel^{1*}

¹ CEMES-CNRS, Université Paul Sabatier, 29 rue Jeanne Marvig, 31055 Toulouse, France

² STMicroelectronics, 820 rue Jean Monnet, 38920 Crolles, France

*Corresponding author

martin.hytch@cemes.fr

christophe.gatel@cemes.fr

ABSTRACT

Electrical resistivity is the key parameter in the active regions of many current nanoscale devices, from memristors to resistive random-access memory and to phase-change memories. The local resistivity of the materials is engineered at the nanoscale to fit the performance requirements. Phase-change memories, for example, rely on materials whose electrical resistance increases dramatically on changing from a crystalline to an amorphous phase. Electrical characterization methods have been developed to measure the response of individual devices but cannot map the local resistance across the active area. Here, we propose a method based on *operando* electron holography to determine the local resistance within working devices. On switching the device, we show that electrical resistance is inhomogeneous on the scale of only a few nanometers.

KEYWORDS Phase change materials, electrical resistivity, *in situ* TEM, *operando* experiments, electron holography, finite element modelling.

MAIN TEXT

The use of electrical resistivity as a parameter to drive devices is receiving increasing attention due to the development of memristors^{1,2}, resistive random-access memory (RRAM) and phase-change memories (PCM).³⁻⁵ Applications range from active components for more energy-efficient machine learning and in-memory computing^{6,7} to emerging photonic applications.^{8,9} Additionally, phase-change memories promise better performance and lower leakage currents than in conventional devices.¹⁰ They depend on materials that exhibit a huge variation in electrical resistance on changes of phase, typically from crystalline to amorphous state. The phase change occurs very locally on the scale of nanometres.

In order to understand the operation of devices, different *in situ* techniques have been developed to monitor the phase transition, notably in transmission electron microscopy (TEM).¹¹ A distinction needs to be made between *in situ* experiments that heat the whole specimen, usually thin films, to provoke the phase change¹²⁻¹⁴ and *operando* experiments that aim to be closer to the actual operation of devices by injecting current pulses *in situ*.^{15,16} However, all depend on

structural or chemical analysis and do not probe directly the local electrical properties. Here we present a method based on *operando* electron holography to determine the local resistance with nanometre spatial resolution. We demonstrate the technique on a working industrial PCM device and reveal the inhomogeneity of the resistivity in the active layer. Beyond the interest for PCM, the technique is applicable to many other devices where changes in local electrical resistance are of primary importance.

Phase-change materials first came to the fore in applications for optical data storage, notably ternary alloys based on Ge-Sb-Te (GST).¹⁷ They exhibit a huge change of optical index and electrical resistivity between the amorphous (high resistance) and crystalline phase (low resistance). Local heating with a laser can induce the phase transformation reversibly. The idea of using these materials as electronic memory came later, with the local heating provided by the flow of current. The electrical resistivity encodes the state of the bit, denoted SET for the crystalline state (low resistance) and RESET for the amorphous state (high resistance). Once the current pulse has passed, no power is required to maintain the state, which makes PCM inherently interesting for low-energy applications. Different designs have been proposed over the years, the “mushroom-type PCM” being one of the most studied.^{17,18}

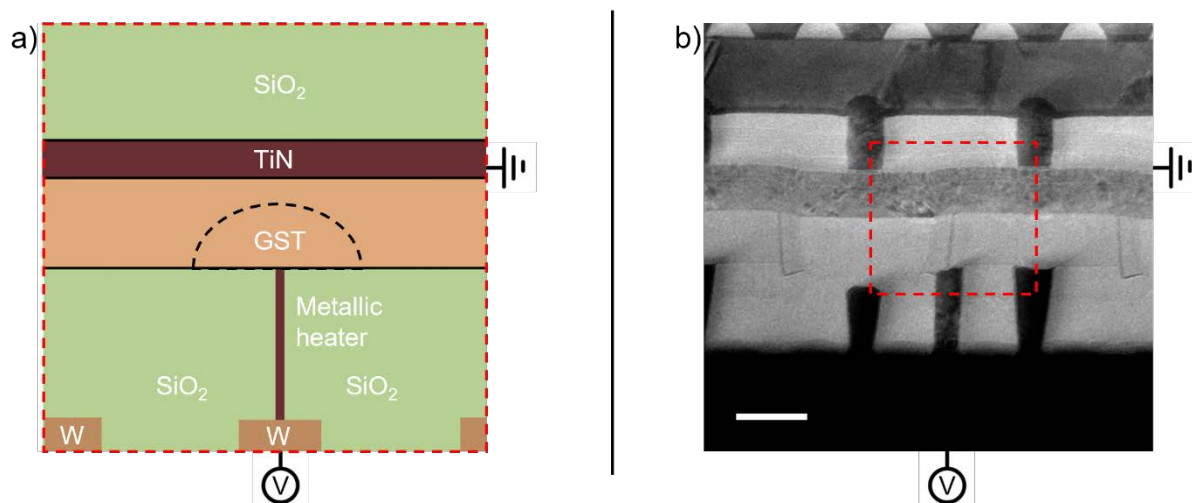


Figure 1. a) Schematic representation of a PCM in a Wall architecture and b) PCM cell studied by *operando* holography. The dotted red rectangle corresponds to the area studied below. Scale bar is 100 nm.

To read the device shown in Figure 1, which is a PCM with a wall-type architecture¹⁹, the resistance is measured by biasing the top and bottom electrode connected to a thin metallic filament called the “heater”. To write, a high-amplitude current pulse is injected, whose exact form depends on whether the operation is to stabilize the crystalline phase (SET) or the amorphous state (RESET). Current passing through the heater and GST layer causes localised Joule heating; the associated rise in temperature in turn causes the phase change. To SET, a relatively long pulse allows gradual crystallisation of the amorphous state whilst for RESET, a short pulse induces rapid melt-quench of the crystalline to amorphous state. The time duration of these electrical pulses never exceeds a few microseconds, , to circumscribe the phase change zone where melting takes place in the immediate vicinity of the heater, creating the dome shape and limiting the diffusion of chemical species. As is easily understandable from the geometry,

the procedure is complex: firstly, the local current depends on the distribution of resistivity within the phase-change layer; secondly, the resulting temperature rise depends additionally on the diffusion coefficients and finally, the local phase change on the temperature, local crystallinity and chemistry. Modelling has to rely on many of the parameters that lack independent experimental verification.²⁰

The electrical characteristics of individual devices can indeed be measured by micro or nano four-point probe techniques²¹ and atomic force microscopy (AFM) where conducting tips can map local resistivity with remarkable spatial resolution even across cross-sectional samples of devices.^{22,23} *In situ* transmission electron microscopy (TEM) can monitor structural and chemical modifications within resistive devices during current flow^{11,24} but measuring changes in resistance within a device during operation is much more challenging. In this paper, we will show how electron holography can be used to measure the local resistivity distribution within the active layer after changing the state *in situ*.

Local resistivity measurement using electron holography

Electron holography has long been used to measure the electrostatic fields in materials, firstly in-built fields across p-n junctions²⁵ and in transistors²⁶ to fields in devices whilst applying bias *in situ*.²⁷⁻³¹ Potentials are interpreted in terms of local charge distributions³² and the sensitivity of electron holography can attain the single elementary charge.^{33,34} In all of these studies, leakage currents were kept to a minimum in order to preserve the specimen from overheating, which can cause catastrophic failure of the nanoscale device, and to maintain the interpretation of the results purely in terms of electrostatics. Here, we prone a different approach and attempt to measure potentials *during* the flow of current. This will allow us to interpret local potential drops in terms of resistivity, the primary property of interest for phase-change materials.

The first successful *in situ* TEM experiments on phase-change materials injected electric pulses in nanowires of GeTe.³⁵ They highlighted the need to encapsulate the material, to avoid germanium evaporation, and the importance of void formation during the phase transformation. To address the question of whether electron radiation influences the phase change, low-dose conditions were chosen and the phase change was induced whilst blanking the beam.³⁶ The technique was further developed to observe switching in real PCM devices.^{15,16,37} To be able to measure the local resistivity with our approach, we additionally need to design specimens compatible with electron holography that can resist the injection of electrical pulses and allow observations during DC current flow.

Electron holography, in off-axis conditions, consists in interfering part of the coherence electron beam passing through the vacuum (the reference wave) with the beam passing through the region of interest (object wave). Whilst primarily used for the study of magnetic and electric fields,³⁸ the dark-field configuration allows the measurement of strain.³⁹ Here, we wish to extend the technique to the quantitative measurement of sample resistivity. This has been suggested previously for contact resistances,⁴⁰ for the study of changes in resistance in resistive random-access memory⁴¹ and to identify conducting precipitates.⁴² However only the potential distribution was studied, without measuring resistivity quantitatively and locally. We follow on from the latter by including quantitative comparison of the phase distribution with finite element method (FEM) modelling to determine the local resistivity in a PCM device.

In the absence of magnetic and strain fields, the phase of the electron hologram in the (x, y) image plane is directly related to the electrostatic potential encountered by the fast electron along its trajectory parallel to the z axis:

$$\phi(x, y) = C_E \int V(x, y, z) dz \quad \text{Equation 1}$$

where C_E depends only on universal constants and the accelerating voltage of the microscope.

Experimentally, the hologram is first recorded with both terminals grounded to determine the phase contribution from the mean-inner potential (MIP) of the material and any fixed charges present. The phase is then measured whilst applying bias and, in our case, as current flows. The two phases are subtracted to obtain the phase change caused only by the biasing. Because of the stray fields above and below the thin lamella, the phase is compared with modelling to determine the electric potential within the sample.³⁰

As mentioned previously, electrostatic modelling only takes into account the charge distribution. In DC conditions, the more appropriate description follows Ohm's law:

$$V = IR \quad (2)$$

where the potential drop across a conductor (V) is given by the current (I) and resistance (R). The local differential form with \mathbf{r} the vector position is:

$$\mathbf{E}(\mathbf{r}) = \rho(\mathbf{r})\mathbf{j}(\mathbf{r}) \quad (3)$$

where the gradient of the potential gives the local electric field, \mathbf{E} , \mathbf{j} the local current density vector and ρ the local resistivity. By modelling the electric potential using this equation to fit the experimental phase, the local electrical resistivity can thus be determined.

To test the new methodology, we chose industrial PCM devices rather than a lab-grown structure, contrary to what might be expected. Indeed, an industrial device already has the electrodes in place and the necessary geometry to supply the localised heating. Furthermore, the device is encapsulated in a protective layer to avoid the problems of Ge evaporation during operation, as mentioned previously. Any results obtained are thus additionally of immediate practical use for understanding performance and possible failure mechanisms for applications.

Nevertheless, a dedicated sample preparation protocol had to be developed to extract a thin lamella suitable for *in situ* electron holography from the wafer whilst preserving the electrical functionality of a single PCM device. The adopted geometry avoids the use of probe-based holders used in previous studies^{16,37} where the stray field around the biased nanotip disturbs the reference area of the hologram⁴², and with possible mechanical and contacting instabilities. The specimen-device is thinned by focused ion-beam (FIB) and contacted to a chip with predefined electrical contacts, similarly to our previous work on electrostatic fields.^{30,31} An important part of the preparation was to preserve the encapsulation layer of insulating material all around the heater and GST layer. Special care was also taken to avoid any electrical discharges which would destroy the device. We limited the total electron dose and we did not observe any beam irradiation effect on the device during the experiment. Figure 1b shows the device that was thinned and contacted for *operando* electron holography experiments (for more details, see the specimen-device preparation part in Supporting Information).

Results

The GST layer within the device is initially crystalline (Initial state) and holograms were first recorded under a low DC bias of 0.5 V as if the memory was to be read. This biasing value for holography observations limits heat effect due to the electrical current. The layer was then switched to an amorphous state (Final state) by sending a sequence of pulses of a few hundreds of nanoseconds. This time duration does not allow observations to be made during phase change. However, remarkably, the thin lamella survived the injection of peak currents of several hundreds of μA during the pulse. As shown in Figure 2a and 2d, conventional TEM contrast due to GST crystalline grains in diffraction conditions disappeared within a dome-like shape around the heater after pulse injection (and see Supporting Information). Once this had occurred, holograms were again recorded in read mode. The overall resistance, measured under a biasing of 0.5 V during the holography experiments, changed radically between the initial and final states, increasing 5-fold after switching.

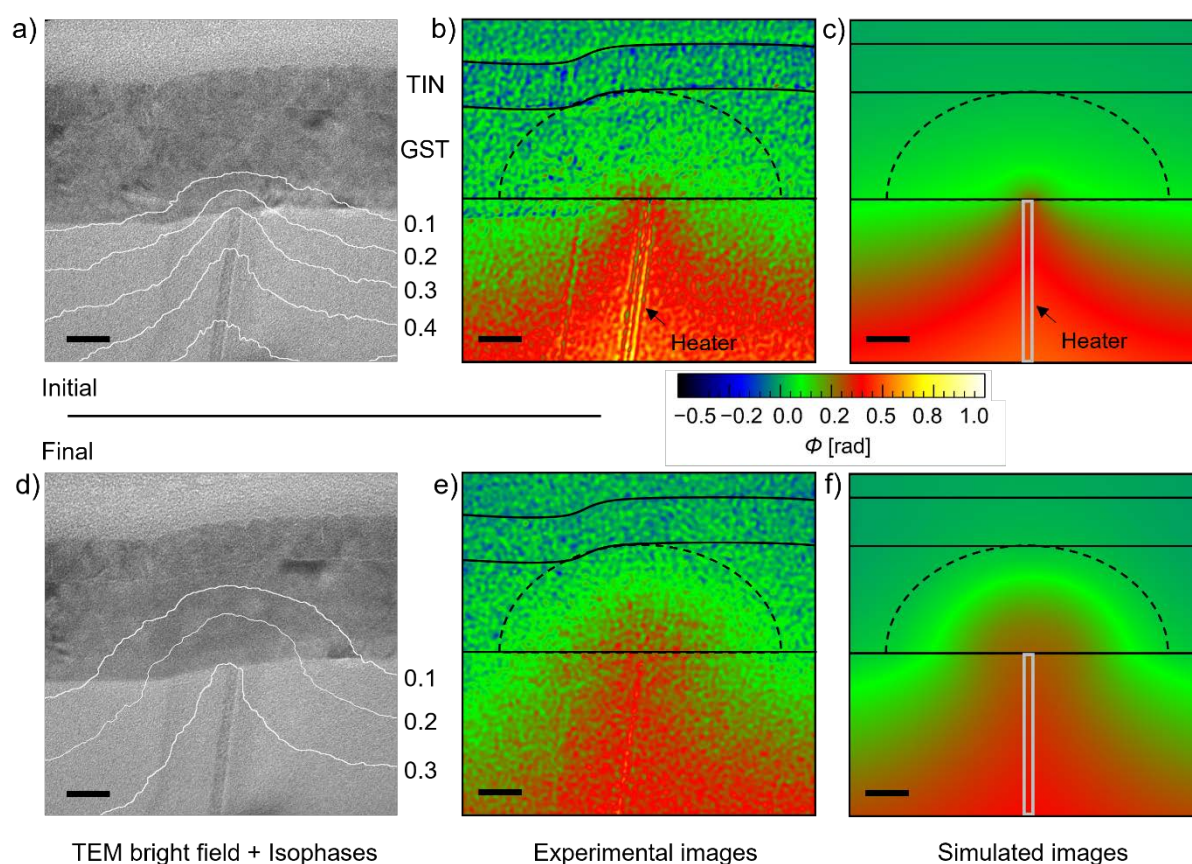


Figure 2. Conventional bright-field TEM image, Initial state (a), Final state (d) with isophase contours (values on the right) extracted from experimental phase maps, Initial (b), Final (e). Simulated phase maps, Initial (c), Final (f). In dotted line the dome-like shape where the phase change occurs. Scale bars are 20 nm.

The corresponding phase images in initial and final states are presented in Figure 2b and 2e, respectively. We can clearly see the difference of the potential distribution between both states, with a dome-like shape in spanning the GST layer in the final state after amorphisation.

However, to obtain this level of phase sensitivity, it was necessary to use extremely long exposure times of four minutes coupled with automated drift compensation.⁴⁴

The electrical information, in the form of isophase contours, has also been superimposed onto the conventional TEM images (Figure 2a and 2d) to help visualise the region involved. We can see, notably, that the phase contours seem to radiate outwards from the tip of the heater into the GST layer. However, the phase maps cannot be directly interpreted quantitatively in terms of the electrical potential within the sample, notably because of the influence of the stray fields around the thin TEM lamella.³⁰ We therefore carried out extensive finite element method (FEM) modelling of the whole device to fit the experimental data (see the simulation details part in Supporting Information). The best fitting phase maps are shown in Figure 2c and 2f alongside the experimental phase maps (Figure 2b and Figure 2e) with exactly the same colour scale. This perfect agreement between the experimental and simulated phase maps gives access using the Equation 1 to the distribution of the electric potential within the device, and therefore to the local resistivity with the Ohm's law.

To help the comparison, experimental and simulated phase profiles in the critical region across the GST layer from the heater to the top electrode are shown in Figure 3. The change on switching from the crystalline to the amorphous state is clearly visible. Interestingly, a uniform conductivity in the GST layer could not reproduce the experimental phase profiles, either the initial or final state, notably in the localisation of the points of inflection and the regions of highest electric field. Therefore, in order to obtain the fit, we found it necessary to vary the conductivity within the GST layer as a function of the distance from the heater (Figure 4).

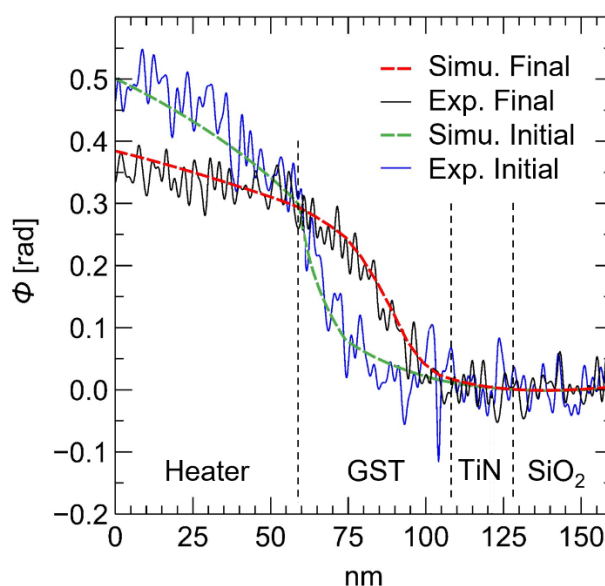


Figure 3. Comparison between experimental and simulated phase profiles for Initial (crystalline) state and Final (amorphous) state.

Discussion

The measurement of the local resistivity is indirect as it relies on the construction of a realistic model to fit the experimental data. We can be confident, nevertheless, in the local electric potential within the sample determined in this way because of the very close relationship between potential and phase (Equation 1). The voltage drop from heater to top electrode measured from the phase image is almost identical to that macroscopically applied voltage for the initial state (0.5 V), which suggests that the contact resistance is minimal. For the final state, there is a slight difference between the local bias determined by the model (0.46 V) and the applied bias (0.5 V), suggesting a contact resistance which may have been caused by the electrical pulses.

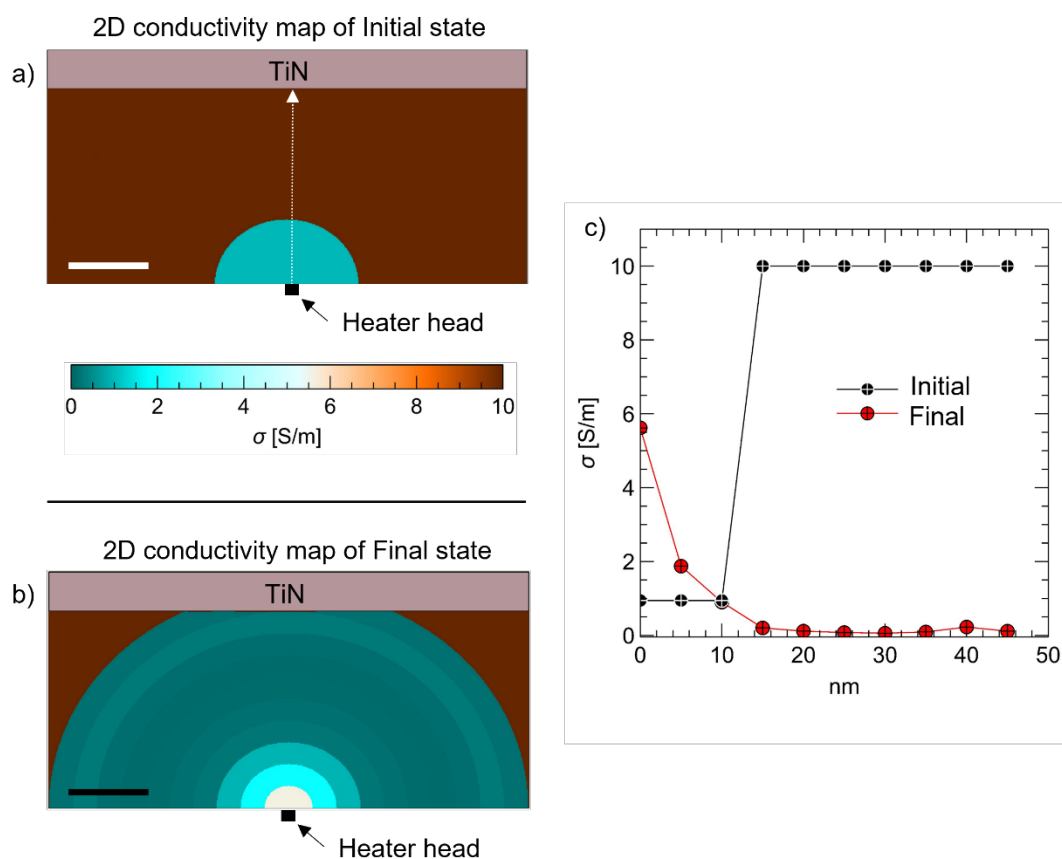


Figure 4. Local conductivity for Initial state (a) and Final state (b) from FEM. The graph in (c) shows the variation of the conductivity across the GST layer. Scale bars are 20 nm.

The local conductivity, however, relies on the internal consistency between the resulting distribution of current and the electric potential. In our case, we have made the reasonable assumption, given the form of the phase contours, that the conductivity is radially symmetric around the heater tip. The absolute value of the conductivity in the model was fixed by the experimentally measured total current flowing through the device *in situ*. We have also assumed that Ohm's law applies locally for this material^{45,46}, which is maybe more questionable.

The increase in overall resistance between the two states is smaller than expected for operational devices. This is because the operational SET state has to be formed through an activation procedure⁴⁷ which has not carried out here. However, the maximum conductivity in the GST

layer in the initial state, presumably the well-crystallised region, is 100 times the minimum conductivity in the final state, presumably fully amorphous, much nearer to the expected values. In view of the inhomogeneous resistivity for both states, we conclude the *in situ* switching was incomplete. Nevertheless, this example shows the power of the technique. A small seed of highly resistive material around the heater tip was revealed in the initial crystalline state and for the final state, the crystalline to amorphous transformation occurred at a certain radius, about 10 nm, from the heater tip. This is probably due to different cooling rates after the injection of the electrical pulse. Indeed, chemical and structural inhomogeneities have already been observed in such devices through post-mortem TEM studies.^{48,49}

Conclusion

We developed a new methodology to map the local resistivity across the active area of an individual device in operation. This method, based on *operando* electron holography, has been applied on a PCM cell in wall architecture and directly highlights unexpected features. On switching the device by electrical pulses, we demonstrated that electrical resistance is inhomogeneous near the heater. The approach presented here is in no way limited to the study of phase-change memory. We propose the technique as general way of identifying and measuring local inhomogeneities in electrical resistance. In principle, there is no reason the technique could not be extended to three-dimensional mapping of electric resistance within materials and devices through tomographic reconstruction, as has been shown for other TEM and electron holography modes.⁵⁰

METHODS

Specimen-device Preparation

Specimens for *operando* electron holography experiments were extracted from production lines of STMicroelectronics and prepared by focused ion beam (FIB). The FIB system used for this specific sample preparation is a Helios G5-FX dual beam system from ThermoFisher, embedding both a FIB and a SEM columns, a micromanipulator and a gas injector (to deposit tungsten layers). Details on this specific sample preparation are given in the specimen-device preparation part in Supporting Information.

The chip supporting the connected devices was inserted into a Hummingbird holder designed specifically for biasing experiments (1600 series, Hummingbird scientific) and connected to this additional setup.

Electron Holography

Operando electron holography experiments were performed on the I2TEM microscope, an Hitachi HF3300-C TEM specially designed for *in situ* electron interferometry experiments, in Lorentz-TL11 mode allowing to reach 0.5 nm of spatial resolution with a large field of view.⁵¹ The reference wave was placed in the field-free region of the vacuum above the top W electrode. Completing the setup is a high-speed 4k by 4k camera (OneView, Gatan Inc.). Holography experiments were performed at an operating voltage of 300 kV ($C_E = 6.526 \times 10^6 \text{ V}^{-1} \cdot \text{m}^{-1}$), elliptical illumination and 2 post-specimen biprisms to allow flexibility in the holographic configurations and to eliminate the Fresnel fringe artefacts.⁵² The camera was functioning at

L. Zhang, F. Lorut, K. Gruel, M.J. Hÿtch, and C. Gatel, **Nano Letters** 24, 5913-5919 (2024).
Measuring electrical resistivity at the nanoscale in phase-change materials. [10.1021/acs.nanolett.4c01462](https://doi.org/10.1021/acs.nanolett.4c01462)

full-frame rate of 25 images per second and temporal integration window of 1 s which corresponds to a sum of the frames displayed in the last second. Holograms with an interfringe of 0.85 nm (8.2 pixels) were acquired using dynamic automation⁴⁴ and the pi-shift method⁵³ over a total exposure time of 240 s (4 mn) each corresponding to the sum of 240 images.

During *operando* electron holography experiments, the DC biasing was provided by Keithley 2635B source meter. The electrical pulses were intriuged from a Keithley 4200A-SCS instrument, equipped with 4225-PMU, CVU, 2 SMU and 2 RPM remote amplifier modules. The timing resolution for the pulsing is 20 ns.

In-house scripts and dedicated code implemented within Digital Micrograph for GMS 3.3 (Gatan Inc.) were used to analyze the holograms and extract amplitude and phase images during post-processing. A 5th order Butterworth Fourier-space filter centered on the sideband giving a spatial resolution of 1.7 nm was selected for the amplitude and phase images. To remove the projector and camera distortion-induced phase modulations, a dedicated reference hologram recorded in a vacuum area during an exposure time of 480 s was used.

Finite Element Modelling

Finite element modelling (FEM) simulations were conducted using COMSOL Multiphysics®, software specifically designed for studying the physical properties of systems, particularly those involving coupled physics problems. The stationary solver was applied to address two physics aspects: simulating the induction, which involves resolving the electrical distribution inside and outside the sample, and solving the electrical circuit.

The model geometry was determined using the amplitude image reconstructed from the electron hologram as reference and information given by the manufacturer. For optimal results and to minimize potential box effects in FEM calculations, boundary conditions at the domain edges were set to infinity. A swept mesh technique was employed to handle the "infinite layer", effectively adapting to the needs of this particular type of calculation. The mesh itself was divided into two main zones to ensure efficient simulation and resource utilization. The software precisely determines the positions of the mesh points, ensuring a highly accurate representation of the geometry of the system and interfaces.

More details on the finite element modelling applied to the PCM device can be found in the Supporting Information.

ACKNOWLEDGEMENTS

This work was supported by the French national project IODA (ANR-17-CE24-0047) and the labex. This study has also been supported through the EUR grant NanoX no. ANR-17-EURE-0009 and the EQUIPEX grant ANR-10-EQPX-38-01 in the framework of the "Programme des Investissements d'Avenir". The research leading to these results has received additional funding from the European Union Horizon 2020 research and innovation programme under grant agreement No. 823717 – ESTEEM3.

ASSOCIATED CONTENT

Supporting Information

L. Zhang, F. Lorut, K. Gruel, M.J. Hÿtch, and C. Gatel, **Nano Letters** 24, 5913-5919 (2024).
Measuring electrical resistivity at the nanoscale in phase-change materials. [10.1021/acs.nanolett.4c01462](https://doi.org/10.1021/acs.nanolett.4c01462)

The supporting information is available of free of charge.

Details on the specimen-device preparation (schematic illustration of FIB-prepared specimen structure, effect of the electrostatic discharge, biasing Hummingbird sample holder and chip supporting the specimen-device, TEM image of the whole specimen-deice containing a single connected PCM cell, bright field TEM images and diffraction patterns at the initial and final states), electron holography experiments (Hitachi HF-3300 microscope, Lorentz-TL11 mode, reference wave area, amplitude and phase images of the whole region) and simulation processing (equation, model used for the FEM calculations, phase fitting method).

AUTHOR INFORMATION

Corresponding Authors

Martin Hÿtch – *CEMES-CNRS, Toulouse, France*

Email: martin.hytch@cemes.fr

Christophe Gatel – *CEMES-CNRS, University of Toulouse, Toulouse, France*

Email: christophe.gatel@cemes.fr

Authors

Leifeng Zhang - *CEMES-CNRS, Toulouse, France*

Frédéric Lorut – *STMicroelectronics, Crolles, France*

Kilian Gruel - *CEMES-CNRS, Toulouse, France*

REFERENCES

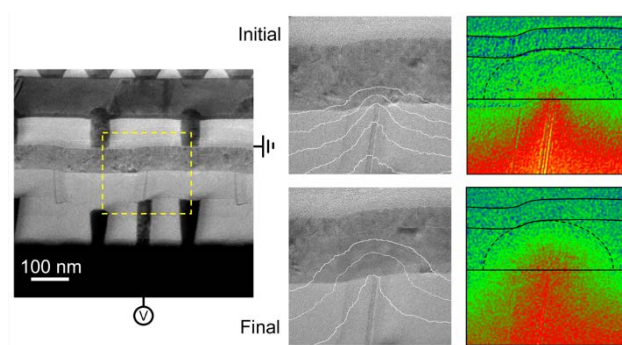
- (1) Yang, J. J.; Strukov, D. B.; Stewart, D. R. Memristive Devices for Computing. *Nat. Nanotechnol.* **2013**, 8 (1), 13–24. <https://doi.org/10.1038/nnano.2012.240>.
- (2) Song, M.-K.; Kang, J.-H.; Zhang, X.; Ji, W.; Ascoli, A.; Messaris, I.; Demirkol, A. S.; Dong, B.; Aggarwal, S.; Wan, W.; Hong, S.-M.; Cardwell, S. G.; Boybat, I.; Seo, J.; Lee, J.-S.; Lanza, M.; Yeon, H.; Onen, M.; Li, J.; Yildiz, B.; del Alamo, J. A.; Kim, S.; Choi, S.; Milano, G.; Ricciardi, C.; Alff, L.; Chai, Y.; Wang, Z.; Bhaskaran, H.; Hersam, M. C.; Strukov, D.; Wong, H.-S. P.; Valov, I.; Gao, B.; Wu, H.; Tetzlaff, R.; Sebastian, A.; Lu, W.; Chua, L.; Yang, J. J.; Kim, J. Recent Advances and Future Prospects for Memristive Materials, Devices, and Systems. *ACS Nano* **2023**, 17 (13), 11994–12039. <https://doi.org/10.1021/acs.nano.3c03505>.
- (3) Bez, R.; Pirovano, A. Non-Volatile Memory Technologies: Emerging Concepts and New Materials. *Mater. Sci. Semicond. Process.* **2004**, 7 (4), 349–355. <https://doi.org/10.1016/j.mssp.2004.09.127>.
- (4) Lankhorst, M. H. R.; Ketelaars, B. W. S. M. M.; Wolters, R. a. M. Low-Cost and Nanoscale Non-Volatile Memory Concept for Future Silicon Chips. *Nat. Mater.* **2005**, 4 (4), 347–352. <https://doi.org/10.1038/nmat1350>.

- L. Zhang, F. Lorut, K. Gruel, M.J. Hÿtch, and C. Gatel, **Nano Letters** 24, 5913-5919 (2024).
Measuring electrical resistivity at the nanoscale in phase-change materials. [10.1021/acs.nanolett.4c01462](https://doi.org/10.1021/acs.nanolett.4c01462)
- (5) Wuttig, M.; Yamada, N. Phase-Change Materials for Rewriteable Data Storage. *Nat. Mater.* **2007**, 6 (11), 824–832. <https://doi.org/10.1038/nmat2009>.
 - (6) Yu, S. Neuro-Inspired Computing with Emerging Nonvolatile Memorys. *Proc. IEEE* **2018**, 106 (2), 260–285. <https://doi.org/10.1109/JPROC.2018.2790840>.
 - (7) Sebastian, A.; Le Gallo, M.; Khaddam-Aljameh, R.; Eleftheriou, E. Memory Devices and Applications for In-Memory Computing. *Nat. Nanotechnol.* **2020**, 15 (7), 529–544. <https://doi.org/10.1038/s41565-020-0655-z>.
 - (8) Wuttig, M.; Bhaskaran, H.; Taubner, T. Phase-Change Materials for Non-Volatile Photonic Applications. *Nat. Photonics* **2017**, 11 (8), 465–476. <https://doi.org/10.1038/nphoton.2017.126>.
 - (9) Feldmann, J.; Youngblood, N.; Karpov, M.; Gehring, H.; Li, X.; Stappers, M.; Le Gallo, M.; Fu, X.; Lukashchuk, A.; Raja, A. S.; Liu, J.; Wright, C. D.; Sebastian, A.; Kippenberg, T. J.; Pernice, W. H. P.; Bhaskaran, H. Parallel Convolutional Processing Using an Integrated Photonic Tensor Core. *Nature* **2021**, 589 (7840), 52–58. <https://doi.org/10.1038/s41586-020-03070-1>.
 - (10) Wuttig, M. Towards a Universal Memory? *Nat. Mater.* **2005**, 4 (4), 265–266. <https://doi.org/10.1038/nmat1359>.
 - (11) Sun, W.; Gao, B.; Chi, M.; Xia, Q.; Yang, J. J.; Qian, H.; Wu, H. Understanding Memristive Switching via in Situ Characterization and Device Modeling. *Nat. Commun.* **2019**, 10 (1), 3453. <https://doi.org/10.1038/s41467-019-11411-6>.
 - (12) D'Arrigo, G.; Mio, A. M.; Boniardi, M.; Redaelli, A.; Varesi, E.; Privitera, S.; Pellegrino, G.; Spinella, C.; Rimini, E. Crystallization Properties of Sb-Rich GeSbTe Alloys by in-Situ Morphological and Electrical Analysis. *Mater. Sci. Semicond. Process.* **2017**, 65, 100–107. <https://doi.org/10.1016/j.mssp.2016.07.014>.
 - (13) Singh, M. K.; Ghosh, C.; Miller, B.; Kotula, P. G.; Tripathi, S.; Watt, J.; Bakan, G.; Silva, H.; Carter, C. B. In Situ TEM Study of Crystallization and Chemical Changes in an Oxidized Uncapped Ge₂Sb₂Te₅ Film. *J. Appl. Phys.* **2020**, 128 (12), 124505. <https://doi.org/10.1063/5.0023761>.
 - (14) Luong, M. A.; Ran, S.; Bernard, M.; Claverie, A. An Experimental Study of Ge Diffusion through Ge₂Sb₂Te₅. *Mater. Sci. Semicond. Process.* **2022**, 152, 107101. <https://doi.org/10.1016/j.mssp.2022.107101>.
 - (15) Xie, Y.; Kim, W.; Kim, Y.; Kim, S.; Gonsalves, J.; BrightSky, M.; Lam, C.; Zhu, Y.; Cha, J. J. Self-Healing of a Confined Phase Change Memory Device with a Metallic Surfactant Layer. *Adv. Mater.* **2018**, 30 (9), 1705587. <https://doi.org/10.1002/adma.201705587>.
 - (16) Oh, S. H.; Baek, K.; Son, S. K.; Song, K.; Oh, J. W.; Jeon, S.-J.; Kim, W.; Yoo, J. H.; Lee, K. J. In Situ TEM Observation of Void Formation and Migration in Phase Change Memory Devices with Confined Nanoscale Ge₂Sb₂Te₅. *Nanoscale Adv.* **2020**, 2 (9), 3841–3848. <https://doi.org/10.1039/D0NA00223B>.
 - (17) Hudgens, S.; Johnson, B. Overview of Phase-Change Chalcogenide Nonvolatile Memory Technology. *MRS Bull.* **2004**, 29 (11), 829–832. <https://doi.org/10.1557/mrs2004.236>.
 - (18) Ding, K.; Wang, J.; Zhou, Y.; Tian, H.; Lu, L.; Mazzarello, R.; Jia, C.; Zhang, W.; Rao, F.; Ma, E. Phase-Change Heterostructure Enables Ultralow Noise and Drift for Memory Operation. *Science* **2019**, 366 (6462), 210–215. <https://doi.org/10.1126/science.aay0291>.

- L. Zhang, F. Lorut, K. Gruel, M.J. Hÿtch, and C. Gatel, **Nano Letters** 24, 5913-5919 (2024).
Measuring electrical resistivity at the nanoscale in phase-change materials. [10.1021/acs.nanolett.4c01462](https://doi.org/10.1021/acs.nanolett.4c01462)
- (19) Servalli, G. A 45nm Generation Phase Change Memory Technology. In *2009 IEEE International Electron Devices Meeting (IEDM)*; 2009; pp 1–4. <https://doi.org/10.1109/IEDM.2009.5424409>.
- (20) Sebastian, A.; Le Gallo, M.; Krebs, D. Crystal Growth within a Phase Change Memory Cell. *Nat. Commun.* **2014**, 5 (1), 4314. <https://doi.org/10.1038/ncomms5314>.
- (21) Bogdanowicz, J.; Folkersma, S.; Sergeant, S.; Schulze, A.; Moussa, A.; Petersen, D. H.; Hansen, O.; Henrichsen, H. H.; Nielsen, P. F.; Vandervorst, W. Width-Dependent Sheet Resistance of Nanometer-Wide Si Fins as Measured with Micro Four-Point Probe. *Phys. Status Solidi A* **2018**, 215 (6), 1700857. <https://doi.org/10.1002/pssa.201700857>.
- (22) Vandervorst, W.; Fleischmann, C.; Bogdanowicz, J.; Franquet, A.; Celano, U.; Paredis, K.; Budrevich, A. Dopant, Composition and Carrier Profiling for 3D Structures. *Mater. Sci. Semicond. Process.* **2017**, 62, 31–48. <https://doi.org/10.1016/j.mssp.2016.10.029>.
- (23) Orji, N. G.; Badaroglu, M.; Barnes, B. M.; Beitia, C.; Bunday, B. D.; Celano, U.; Kline, R. J.; Neisser, M.; Obeng, Y.; Vladar, A. E. Metrology for the next Generation of Semiconductor Devices. *Nat. Electron.* **2018**, 1 (10), 532–547. <https://doi.org/10.1038/s41928-018-0150-9>.
- (24) Zhang, Y.; Wang, C.; Wu, X. Review of Electrical Stimulus Methods of in Situ Transmission Electron Microscope to Study Resistive Random Access Memory. *Nanoscale* **2022**, 14 (27), 9542–9552. <https://doi.org/10.1039/D2NR01872A>.
- (25) Frabboni, S.; Matteucci, G.; Pozzi, G. Observation of Electrostatic Fields by Electron Holography: The Case of Reverse-Biased p-n Junctions. *Ultramicroscopy* **1987**, 23 (1), 29–37. [https://doi.org/10.1016/0304-3991\(87\)90224-5](https://doi.org/10.1016/0304-3991(87)90224-5).
- (26) Rau, W. D.; Schwander, P.; Baumann, F. H.; Höppner, W.; Ourmazd, A. Two-Dimensional Mapping of the Electrostatic Potential in Transistors by Electron Holography. *Phys. Rev. Lett.* **1999**, 82 (12), 2614–2617. <https://doi.org/10.1103/PhysRevLett.82.2614>.
- (27) Twitchett, A. C.; Dunin-Borkowski, R. E.; Midgley, P. A. Quantitative Electron Holography of Biased Semiconductor Devices. *Phys. Rev. Lett.* **2002**, 88 (23), 238302. <https://doi.org/10.1103/PhysRevLett.88.238302>.
- (28) Ikarashi, N.; Takeda, H.; Yako, K.; Hane, M. In-Situ Electron Holography of Surface Potential Response to Gate Voltage Application in a Sub-30-Nm Gate-Length Metal-Oxide-Semiconductor Field-Effect Transistor. *Appl. Phys. Lett.* **2012**, 100 (14), 143508. <https://doi.org/10.1063/1.3700723>.
- (29) Aizawa, Y.; Yamamoto, K.; Sato, T.; Murata, H.; Yoshida, R.; Fisher, C. A. J.; Kato, T.; Iriyama, Y.; Hirayama, T. In Situ Electron Holography of Electric Potentials inside a Solid-State Electrolyte: Effect of Electric-Field Leakage. *Ultramicroscopy* **2017**, 178, 20–26. <https://doi.org/10.1016/j.ultramic.2016.07.015>.
- (30) Gatel, C.; Serra, R.; Gruel, K.; Masseboeuf, A.; Chapuis, L.; Cours, R.; Zhang, L.; Warot-Fonrose, B.; Hÿtch, M. J. Extended Charge Layers in Metal-Oxide-Semiconductor Nanocapacitors Revealed by Operando Electron Holography. *Phys. Rev. Lett.* **2022**, 129 (13), 137701. <https://doi.org/10.1103/PhysRevLett.129.137701>.
- (31) Brodovoi, M.; Gruel, K.; Masseboeuf, A.; Chapuis, L.; Hÿtch, M.; Lorut, F.; Gatel, C. Mapping Electric Fields in Real Nanodevices by Operando Electron Holography. *Appl. Phys. Lett.* **2022**, 120 (23), 233501. <https://doi.org/10.1063/5.0092019>.
- (32) Beleggia, M.; Kasama, T.; Dunin-Borkowski, R. E.; Hofmann, S.; Pozzi, G. Direct Measurement of the Charge Distribution along a Biased Carbon Nanotube Bundle Using

- L. Zhang, F. Lorut, K. Gruel, M.J. Hÿtch, and C. Gatel, **Nano Letters** 24, 5913-5919 (2024).
Measuring electrical resistivity at the nanoscale in phase-change materials. [10.1021/acs.nanolett.4c01462](https://doi.org/10.1021/acs.nanolett.4c01462)
- Electron Holography. *Appl. Phys. Lett.* **2011**, 98 (24), 243101.
<https://doi.org/10.1063/1.3598468>.
- (33) Gatel, C.; Lubk, A.; Pozzi, G.; Snoeck, E.; Hÿtch, M. Counting Elementary Charges on Nanoparticles by Electron Holography. *Phys. Rev. Lett.* **2013**, 111 (2), 025501.
<https://doi.org/10.1103/PhysRevLett.111.025501>.
- (34) Aso, R.; Hojo, H.; Takahashi, Y.; Akashi, T.; Midoh, Y.; Ichihashi, F.; Nakajima, H.; Tamaoka, T.; Yubuta, K.; Nakanishi, H.; Einaga, H.; Tanigaki, T.; Shinada, H.; Murakami, Y. Direct Identification of the Charge State in a Single Platinum Nanoparticle on Titanium Oxide. *Science* **2022**, 378 (6616), 202–206. <https://doi.org/10.1126/science.abq5868>.
- (35) Meister, S.; Schoen, D. T.; Topinka, M. A.; Minor, A. M.; Cui, Y. Void Formation Induced Electrical Switching in Phase-Change Nanowires. *Nano Lett.* **2008**, 8 (12), 4562–4567.
<https://doi.org/10.1021/nl802808f>.
- (36) Meister, S.; Kim, S.; Cha, J. J.; Wong, H.-S. P.; Cui, Y. In Situ Transmission Electron Microscopy Observation of Nanostructural Changes in Phase-Change Memory. *ACS Nano* **2011**, 5 (4), 2742–2748. <https://doi.org/10.1021/nn1031356>.
- (37) Baek, K.; Song, K.; Son, S. K.; Oh, J. W.; Jeon, S.-J.; Kim, W.; Kim, H. J.; Oh, S. H. Microstructure-Dependent DC Set Switching Behaviors of Ge–Sb–Te-Based Phase-Change Random Access Memory Devices Accessed by in Situ TEM. *NPG Asia Mater.* **2015**, 7 (6), e194–e194. <https://doi.org/10.1038/am.2015.49>.
- (38) Dunin-Borkowski, R. E.; Kovács, A.; Kasama, T.; McCartney, M. R.; Smith, D. J. Electron Holography. In *Springer Handbook of Microscopy*; Hawkes, P. W., Spence, J. C. H., Eds.; Springer Handbooks; Springer International Publishing: Cham, 2019; pp 767–818.
https://doi.org/10.1007/978-3-030-00069-1_16.
- (39) Hÿtch, M.; Houdellier, F.; Hue, F.; Snoeck, E. Nanoscale Holographic Interferometry for Strain Measurements in Electronic Devices. *Nature* **2008**, 453 (7198), 1086–1089.
<https://doi.org/10.1038/nature07049>.
- (40) Takeguchi, M.; Shimojo, M.; Tanaka, M.; Che, R.; Zhang, W.; Furuya, K. Electron Holographic Study of the Effect of Contact Resistance of Connected Nanowires on Resistivity Measurement. *Surf. Interface Anal.* **2006**, 38 (12–13), 1628–1631.
<https://doi.org/10.1002/sia.2403>.
- (41) Li, C.; Gao, B.; Yao, Y.; Guan, X.; Shen, X.; Wang, Y.; Huang, P.; Liu, L.; Liu, X.; Li, J.; Gu, C.; Kang, J.; Yu, R. Direct Observations of Nanofilament Evolution in Switching Processes in HfO₂-Based Resistive Random Access Memory by In Situ TEM Studies. *Adv. Mater.* **2017**, 29 (10), 1602976. <https://doi.org/10.1002/adma.201602976>.
- (42) Kawamoto, N.; Ono, H.; Terasaki, Y.; Fujikawa, Y.; Murakami, Y.; Shindo, D. *In-Situ* Electric Field Observation of Small Precipitates in BaTiO₃ Multilayer Ceramic Capacitors. *Mater. Trans.* **2019**, 60 (10), 2109–2113. <https://doi.org/10.2320/matertrans.MI201902>.
- (43) de Knoop, L.; Houdellier, F.; Gatel, C.; Masseboeuf, A.; Monthieux, M.; Hÿtch, M. Determining the Work Function of a Carbon-Cone Cold-Field Emitter by in Situ Electron Holography. *Micron*. <https://doi.org/10.1016/j.micron.2014.03.005>.
- (44) Gatel, C.; Dupuy, J.; Houdellier, F.; Hÿtch, M. J. Unlimited Acquisition Time in Electron Holography by Automated Feedback Control of Transmission Electron Microscope. *Appl. Phys. Lett.* **2018**, 113 (13), 133102. <https://doi.org/10.1063/1.5050906>.

- L. Zhang, F. Lorut, K. Gruel, M.J. Hÿtch, and C. Gatel, **Nano Letters** 24, 5913-5919 (2024).
Measuring electrical resistivity at the nanoscale in phase-change materials. [10.1021/acs.nanolett.4c01462](https://doi.org/10.1021/acs.nanolett.4c01462)
- (45) Pigot, C.; Bocquet, M.; Gilibert, F.; Reyboz M.; Cueto, O.; Della Marca, V.; Zuliani P.; Portal, J. M. Comprehensive phase-change memory compact model for circuit simulation. *IEEE Transactions on Electron Devices* **2018**, *65*, 4282-4289
<https://doi.org/10.1109/TED.2018.2862155>.
- (46) Giannopoulos, I.; Sebastian, A.; Le Gallo, M.; Jonnalagadda, V. P.; Sousa, M.; Boon, M. N.; Eleftheriou, E. 8-bit precision in-memory multiplication with projected phase-change memory. *IEEE International Electron Devices Meeting (IEDM)* **2018**, pp. 27.7.1-27.7.4, San Francisco, CA, USA
<https://doi.org/10.1109/IEDM.2018.8614558>.
- (47) Sousa, V.; Navarro, G.; Castellani, N.; Coué, M.; Cueto, O.; Sabbione, C.; Noé, P.; Perniola, L.; Blonkowski, S.; Zuliani, P.; Annunziata, R. Operation Fundamentals in 12Mb Phase Change Memory Based on Innovative Ge-Rich GST Materials Featuring High Reliability Performance. In *2015 Symposium on VLSI Technology (VLSI Technology)*; 2015; pp T98–T99.
<https://doi.org/10.1109/VLSIT.2015.7223708>.
- (48) Palumbo, E.; Zuliani, P.; Borghi, M.; Annunziata, R. Forming Operation in Ge-Rich GexSbyTez Phase Change Memories. *Solid-State Electron.* **2017**, *133*, 38–44.
<https://doi.org/10.1016/j.sse.2017.03.016>.
- (49) Henry, L.; Bernier, N.; Jacob, M.; Navarro, G.; Clément, L.; Rouvière, J.-L.; Robin, E. Studying Phase Change Memory Devices by Coupling Scanning Precession Electron Diffraction and Energy Dispersive X-Ray Analysis. *Acta Mater.* **2020**, *201*, 72–78.
<https://doi.org/10.1016/j.actamat.2020.09.033>.
- (50) Midgley, P. A.; Dunin-Borkowski, R. E. Electron Tomography and Holography in Materials Science. *Nat. Mater.* **2009**, *8* (4), 271–280. <https://doi.org/10.1038/nmat2406>.
- (51) Snoeck, E.; Houdellier, F.; Taniguch, Y.; Masseur, A.; Gatel, C.; Nicolai, J.; Hÿtch, M. Off-Axial Aberration Correction Using a B-COR for Lorentz and HREM Modes. *Microsc. Microanal.* **2014**, *20* (S3), 932–933. <https://doi.org/10.1017/S1431927614006382>.
- (52) Harada, K.; Tonomura, A.; Togawa, Y.; Akashi, T.; Matsuda, T. Double-Biprism Electron Interferometry. *Appl. Phys. Lett.* **2004**, *84* (17), 3229–3231.
<https://doi.org/10.1063/1.1715155>.
- (53) Volkov, V. V.; Han, M. G.; Zhu, Y. Double-Resolution Electron Holography with Simple Fourier Transform of Fringe-Shifted Holograms. *Ultramicroscopy* **2013**, *134*, 175–184.
<https://doi.org/10.1016/j.ultramic.2013.06.018>.



TOC Graphic